High-time-resolution Photometry of AR Scorpii: Confirmation of the White Dwarf's Spin-down

Robert A. Stiller[1] , Colin Littlefield[1] , Peter Garnavich[1] , Charlotte Wood[1] , Franz-Josef Hambsch[2,3,4], and Gordon Myers[5,6]

[1] Department of Physics, University of Notre Dame, Notre Dame, IN 46556, USA; rstiller@alumni.nd.edu
[2] AAVSO/Vereniging Voor Sterrenkunde (VVS), Brugge, Belgium
[3] Bundesdeutsche Arbeitsgemeinschaft für Veränderliche Sterne e.V. (BAV), Berlin, Germany
[4] CBA Mol, Belgium
[5] Center for Backyard Astrophysics, San Mateo, USA
[6] AAVSO, 5 Inverness Way, Hillsborough, CA, USA

Abstract

The unique binary AR Scorpii consists of an asynchronously rotating, magnetized white dwarf (WD) that interacts with its red-dwarf companion to produce a large-amplitude, highly coherent pulsation every 1.97 minutes. Over the course of two years, we obtained 39 hours of time-resolved, optical photometry of AR Sco at a typical cadence of 5 s to study this pulsation. We find that it undergoes significant changes across the binary orbital period and that its amplitude, phase, and waveform all vary as a function of orbital phase. We show that these variations can be explained by constructive and destructive interference between two periodic, double-peaked signals: the spin–orbit beat pulse, and a weaker WD spin pulse. Modeling of the light curve indicates that in the optical, the amplitude of the primary spin pulse is 50% of the primary beat amplitude, while the secondary maxima of the beat and spin pulses have similar amplitudes. Finally, we use our timings of the beat pulses to confirm the presence of the disputed spin-down of the WD. We measure a beat-frequency derivative of $\dot{\nu} = (-5.14 \pm 0.32) \times 10^{-17}$ Hz s^{-1} and show that this is attributable to the spin-down of the WD. This value is approximately twice as large as the estimate from Marsh et al. but is nevertheless consistent with the constraints established in Potter & Buckley. Our precise measurement of the spin-down rate confirms that the decaying rotational energy of the magnetized WD is sufficient to power the excess electromagnetic radiation emitted by the binary.

Key words: binaries: close – novae, cataclysmic variables – stars: individual (AR Sco) – stars: magnetic field – white dwarfs

Supporting material: data behind figure, machine-readable table

1. Introduction

The cataclysmic variable AR Scorpii (AR Sco) shows large-amplitude, highly periodic pulsations across the electromagnetic spectrum every 1.97 minutes, superimposed upon a strong waveform at the system's 3.56-hr orbital period (Marsh et al. 2016). The system's low X-ray luminosity rules out the presence of significant accretion by the white dwarf (WD) primary from its M-dwarf companion, so neither of these signals is powered by accretion (Marsh et al. 2016; Takata et al. 2018). Instead, AR Sco has been called a white-dwarf pulsar because its pulsations consist of synchrotron radiation and are apparently powered by the spin-down of its highly magnetized ($\lesssim$500 MG) WD, similar to neutron-star pulsars (Marsh et al. 2016; Buckley et al. 2017).

The spin-down of the WD is a foundational conclusion from Marsh et al. (2016), who calculated that the spin-down rate they detected is large enough to power AR Sco's pulsations. However, Potter & Buckley (2018) contested the significance of this spin-down after finding that the Marsh et al. (2016) spin-down ephemeris did not accurately predict the frequencies of the spin and orbital periods in their optical photometry. Although Potter & Buckley (2018) concluded that a linear spin ephemeris accurately described their data, they were also careful to note that their result constrained—but did not rule out—the WD spin-down. An unambiguous detection of the slowing spin rate, they wrote, would require additional observations.

AR Sco's light curve contains a number of remarkable features at different timescales. The orbital waveform is brightest at phase ∼0.4 and has a peak-to-peak amplitude of ∼1.5–2 mag in the optical, depending on the bandpass. Katz (2017) proposes two alternative models to explain the orbital modulation and why it does not peak at superior conjunction. To provide observational constraints for these models, Littlefield et al. (2017) analyzed archival, ground-based photometry as well as 79 days of continuous photometry by the *Kepler K2* mission. They reported that while the system's overall brightness has remained relatively stable since 2005, the orbital waveform peaked at a different phase and had a slightly lower amplitude between 2005 and 2007. Moreover, the *K2* photometry showed aperiodic brightness fluctuations at the level of a few percent on a timescale of days (Littlefield et al. 2017).

The 1.97-minute pulsations are arguably AR Sco's defining observational characteristic and are remarkable for their speed, amplitude (a factor of ∼4 in the optical), and phase coherence across a wide range of wavelengths, including radio, near-infrared, optical, ultraviolet (Marsh et al. 2016; Stanway et al. 2018) and even soft X-rays (Takata et al. 2018). Their period corresponds with the beat period (i.e., the orbital sideband) between the binary orbital period and 1.95-minute WD spin period, and they are thought to originate on the inner hemisphere of the M5-class companion star (Marsh et al. 2016; Takata et al. 2018). Geng et al. (2016) proposes that the WD's magnetic axis is inclined with

Table 1
Log of SLKT Observations

UT Start Date	Length (hr)	Cadence (s)
2016 Jul 28	2.0	6
2016 Aug 03	1.6	5
2016 Aug 22	0.9	5
2016 Aug 23	1.1	5
2016 Sep 01	1.0	5
2016 Sep 02	0.9	5
2016 Sep 03	0.7	4
2016 Sep 04	0.7	4
2017 Apr 23	2.9	5
2017 May 07	2.3	5
2017 May 08	1.8	5
2017 May 15	1.0	5
2017 May 17	1.9	5
2017 Jun 01	3.1	5
2017 Jun 02	2.1	5
2017 Jun 03	0.8	4
2017 Jul 07	1.6	5
2017 Aug 12	0.9	5
2018 Feb 26	1.4	5
2018 Mar 18	1.0	5
2018 Mar 25	1.7	7
2018 Mar 26	2.8	5
2018 Apr 18	1.3	5
2018 Apr 21	0.8	5
2018 May 24	2.5	5

respect to its rotational axis and that the pulses are caused by the interaction of the WD's magnetosphere with the secondary's wind.

The 1.95-minute spin period of the WD in AR Sco is extremely short when compared with the system's orbit. WDs are not born spinning so rapidly, and it is thought that a phase of high accretion powered AR Sco's rapid spin-up, followed by the current epoch of little or no mass transfer (Marsh et al. 2016; Buckley et al. 2017).

Here, we present high-cadence photometry with the twin objectives of (1) searching for a spin-down and (2) disentangling the spin and beat periods.

2. Data

2.1. SLKT Observations

We obtained 39 hr of high-time-resolution photometry of AR Sco using the 80 cm Sarah L. Krizmanich Telescope (SLKT) and an unfiltered Santa Barbara Instrument Group STL-1001 CCD camera at the University of Notre Dame in 2016, 2017, and 2018. As indicated in Table 1, which lists details of each time series, the exposure time was 2 s, and factoring in the overhead between images, the typical cadence was 5–6 s, and each time series usually spanned 1–3 hr. Figure 1 plots a representative, 2.5-hr long light curve and zooms in on one segment during which the pulsations were especially prominent.

The system's optical pulsations are extremely fast and well-defined, so CCD data must be well-timed in order to be useful. Consequently, we synchronized the clock of the CCD control computer to an atomic clock prior to the start of each time series. Additionally, we measured the shutter lag of the detector (the time offset between the shutter actuation and the timestamp recorded in the FITS header), found it to be stable from night-to-night, and applied an appropriate correction to

the image timestamps. Finally, we applied a BJD_{TDB} correction to all observations using routines in Astropy (Astropy Collaboration et al. 2013).

We used aperture photometry to extract AR Sco's light curve, but there were no optimal comparison stars within the field of view. According to APASS photometry, each of the field stars is quite red, probably because there is a dark nebula associated with the ρ Ophiuchi complex along the line of sight to AR Sco. Faced with this paucity of choices, we selected UCAC4 336-082341 ($\alpha_{2000} = 16^h 22^m 06^s.481$, $\delta_{2000} = -22°53'27''.84$, $g'-r' = 2.17$) as our comparison star. Since the spectral properties of such a reddened star are likely a poor match for those of AR Sco, any attempt to infer standard V magnitudes from the unfiltered photometry would probably suffer from serious systematic errors. Consequently, we do not place our photometry on a standard magnitude scale.

2.2. AAVSO Observations

As indicated in Table 2, coauthors F.J.H. and G.M. observed AR Sco and submitted their observations to the AAVSO International Database[7] under AAVSO observer codes HMB and MGW, respectively. Their observations had cadences that ranged from 14 to 35 s.

3. Analysis

Lomb–Scargle power spectra of the SLKT data, presented in Figure 2, show that the measured spin and beat frequencies agree with those reported in Potter & Buckley (2018). However, the predicted spin and beat frequencies from the Marsh et al. (2016) spin-down ephemeris are in poor agreement with the peaks observed in our data, confirming the result in Potter & Buckley (2018). We explore this issue in depth in Section 4.

After eliminating a small number of SLKT observations with a signal-to-noise ratio (S/N) of less than 5, we display our photometry in Figure 3. The data have been phased to the orbital period based on the ephemeris in Marsh et al. (2016). The zero point of the orbital phase is defined as the moment that the red secondary star is at inferior conjunction. The overall light curve shape is similar to the slower cadence data analyzed by Littlefield et al. (2017). The light curve is asymmetric, with a quick rise to maximum brightness at an orbital phase of 0.4 and a second peak at an orbital phase of ∼0.75.

We assume that the observed light curve can be represented as the sum of a slowly varying orbital modulation and the high-frequency, pulsed emission. To remove the variations associated with the orbit, we divided the orbit into phase bins and identified the faintest 5% of the points in each bin. Because contamination by the pulsed emission inflates the amplitude of the orbital waveform in a simple Lomb–Scargle power spectrum, the faintest observations in these bins more accurately describe the underlying orbital modulation, and we selected the exact threshold from trial-and-error. We then represented these points with a Fourier series so that we could predict the strength of the orbital modulation as a function of orbital phase. As seen in Figure 3, the orbital variation is moderately asymmetric, with the peak brightness just before phase 0.5 and the minimum at phase 0.0.

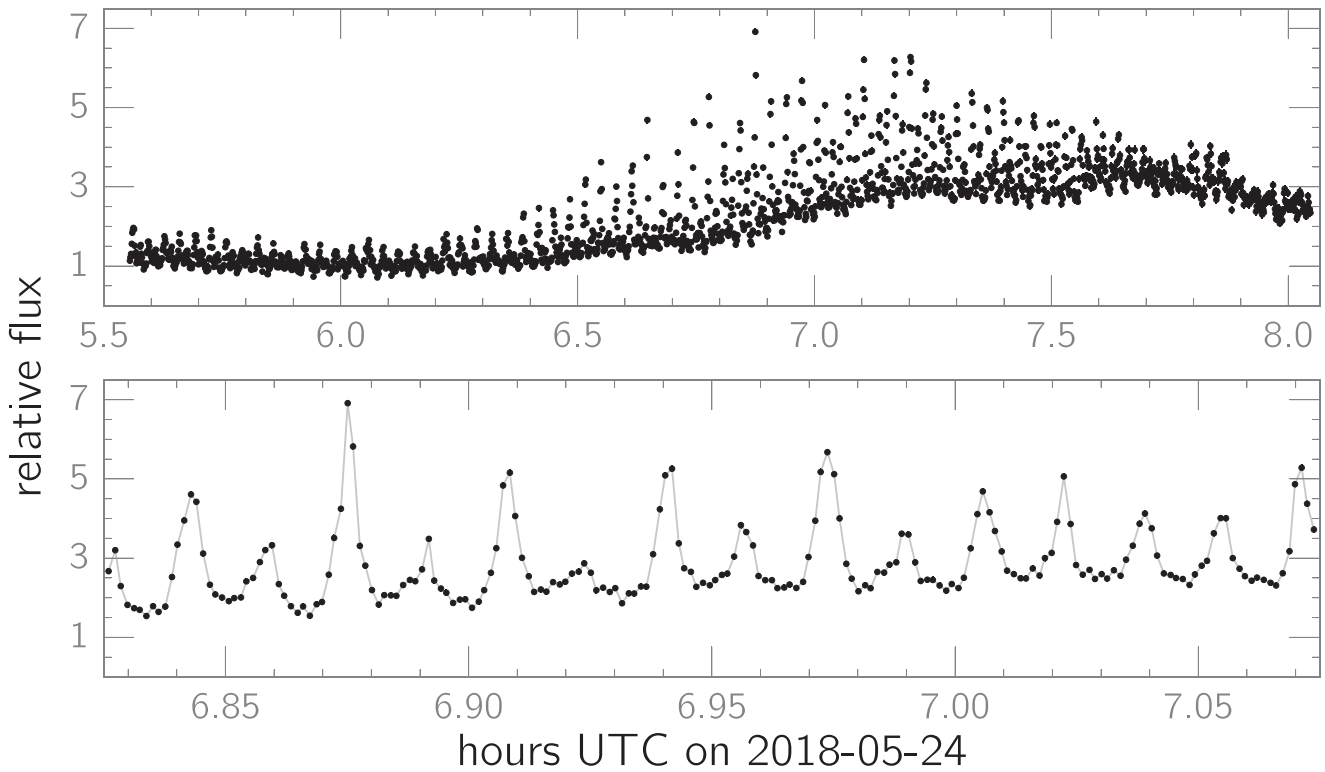---

Figure 1. Sample SLKT light curve of AR Sco. The lower panel replots one section of the upper panel so that the pulsations may be seen more distinctly. The data used to create this figure are available.

Table 2
Log of AAVSO Observations

Observer	UT Start Date	Length (hr)	Cadence (s)
HMB	2015 Jul 24	1.7	35
HMB	2015 Jul 25	4.2	35
HMB	2015 Jul 26	4.3	35
HMB	2015 Jul 27	4.2	35
HMB	2015 Aug 07	2.7	35
HMB	2015 Aug 08	2.3	35
HMB	2015 Aug 10	2.1	35
HMB	2016 Apr 28	4.8	34
HMB	2016 Apr 29	5.7	24
HMB	2016 Apr 30	5.8	24
HMB	2016 May 01	5.9	24
HMB	2016 May 02	5.2	24
HMB	2016 May 03	5.7	24
HMB	2016 May 04	5.7	24
HMB	2016 May 05	5.8	14
HMB	2016 Jul 31	2.6	35
MGW	2016 Aug 05	4.1	24
MGW	2016 Aug 16	2.3	19
MGW	2016 Sep 04	3.7	23
HMB	2016 Sep 09	2.7	35
HMB	2016 Sep 10	2.6	35

Note. The "Obs." column contains the AAVSO code of the observer.

Subtracting the orbital-modulation function from the phased orbital light curve yields the pulsed light curve as a function of orbital phase (bottom panel in Figure 3). The pulse amplitude displays a strong orbital-phase dependence, peaking at orbital phase ∼0.25, reaching minimum amplitude near phase ∼0.6, and rebounding around phase 0.75.

To more closely investigate the changes in the pulse amplitude and morphology, we split the data into 10 equally sized, non-overlapping orbital bins and phased each bin to the beat period. The resulting plots (Figure 4) show that the beat pulse has two unequal maxima per cycle, as has been noted by Marsh et al. (2016). Our beat phase plots show that the shape, amplitude, and phase of both maxima vary as a function of orbital phase. At orbital phase 0.0, the major pulse is broad and symmetric, but between orbital phases 0.1–0.3, its shape changes, with the rise to beat maximum becoming longer than the decline. This is also the orbital phase when the major pulse has the largest amplitude. Around orbital phase 0.35, the major peak is again symmetric but soon skews in the other direction. Eventually, the major peak nearly disappears around phase 0.55. For the second half of the orbit, the major pulse remains symmetrical, but is weaker than in the first half of the orbit. The minor pulse reaches its largest amplitude between orbital phases 0.3 and 0.4, significantly later than phase 0.25 for the major pulse.

The beat pulse undergoes a significant phase shift, depending on the orbital phase. This is most easily seen in a heat map of the pulse brightness versus both the orbital and beat phase (see Figure 5). This figure clearly shows that between orbital phases 0.1 and 0.5, the major peak shifts by 10% in beat phase. The shift in the beat pulse over the second half of the orbit is smaller than the first half, but the pulse is generally seen to be broader and fainter. Takata et al. (2018) reported similar findings from their analysis of 39 ks of data obtained on 2016 September 19 with the *XMM-Newton* satellite's Optical/UV Monitor Telescope, and our results imply that this behavior is stable on timescales of years.
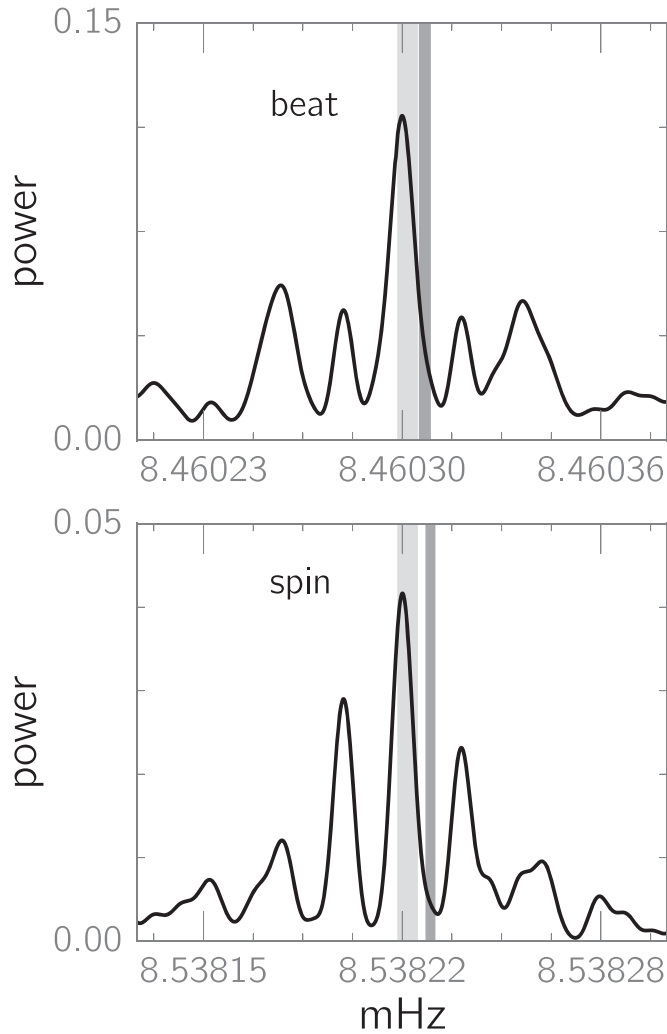
Figure 2. Lomb–Scargle power spectra of the SLKT data, focused on the beat and spin frequencies. The Lomb–Scargle model for both power spectra used two harmonic terms. The light contour gives the 1σ confidence interval from Potter & Buckley (2018), while the dark contour is the projected confidence interval from the spin-down ephemeris Marsh et al. (2016).

Figure 3. Top panel: the light curve of AR Sco phased on the system's orbital period. The scatter results from the ~2-minute periodic flashes that are incoherent at this phasing. The green line is a Fourier series with three harmonics that traces the base of these pulsations, and it represents the orbital modulation in the absence of pulsations. Bottom panel: the residuals after subtraction of the orbital modulation. The amplitude of the pulsed variation peaks at orbital phases ~0.25 and ~0.75.
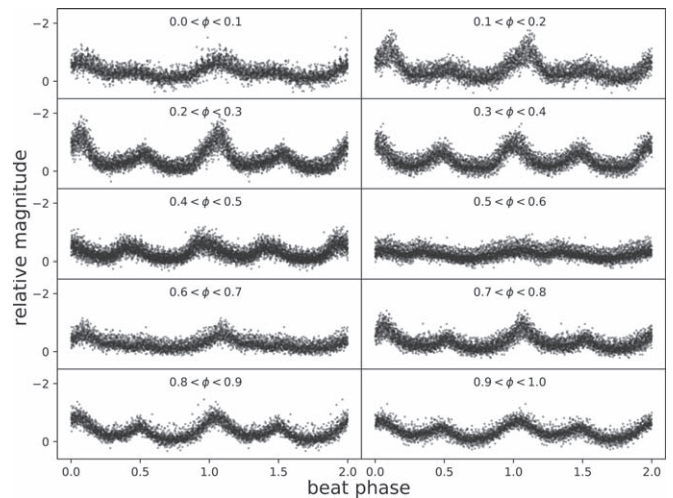
Figure 4. The beat pulse shape as a function of orbital phase. After subtracting the orbital modulation, the light curve was divided into ten orbital phase bins, and each bin is phased on the beat period. Two beat cycles are shown in each panel. Two unequal amplitude peaks are seen each beat cycle suggesting that both poles of the WD magnetic field are interacting with the secondary star. The amplitude and pulse shape are seen to vary with orbital phase. The pulse shape is asymmetric during the first half of an orbit, resulting in its centroid shifting in phase by over 10 s over an orbit.

The amplitude and phase shifts of the beat pulse are consistent with the addition of second periodic signal with a slightly different frequency (e.g., as observed in FO Aqr; Osborne & Mukai 1989). For example, if the spin pulse were to be isolated and plotted in the heat map in Figure 5, it would run diagonally since the figure phases the data to the beat period. To explore this possibility, we modeled the full light curve as the superposition of three periodic signals: the spin, beat, and orbital periods (similar to the light curve model for FO Aqr in its low state (Littlefield et al. 2016)). We found the best-fit trigonometric function at each of those frequencies by a simple least-squares fit, with each term consisting of three harmonics. We also attempted to fit additional frequencies detected in the power spectrum, but adding these terms did not significantly improve the quality of the fit.

The results of this fit (Figure 6) reveal that the beat and spin models are both double-peaked, with the beat pulse having two unequal maxima. The maxima of the spin pulse, by contrast, are roughly equal. Our model predicts that the amplitude of the spin pulse is about 50% of the amplitude of the beat pulse, while the minor pulses are comparable in brightness. However, one limitation of our model is that it underestimates the
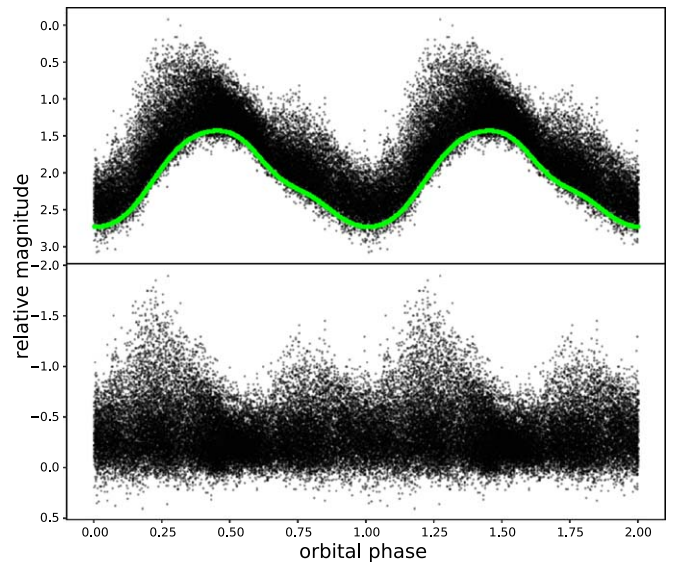
amplitude of the highest-amplitude beat pulses. This might be a consequence of the fact that the model does not account for the changing visibility of the secondary's inner hemisphere across the orbital period.

As a test of this model, we computed the O−C for the blended spin-beat pulse, and as shown in Figure 7, it offers a reasonably accurate prediction of the actual O−C. The simulated O−C includes a correction for light-travel delays caused by the secondary's orbital motion. The light-travel delay for pulsations originating from material orbiting in the plane of
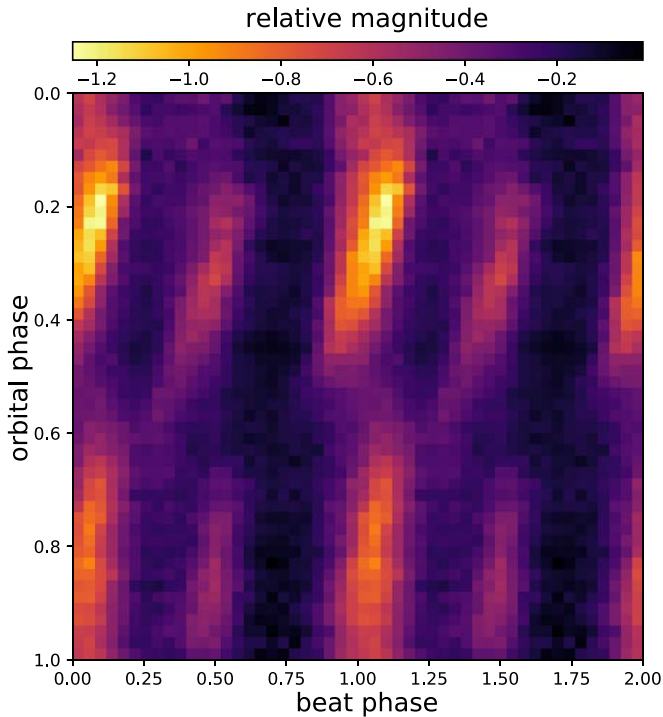
relative magnitude

Figure 5. The AR Sco light curve phased on the beat period as it varies over a binary orbit. The orbital waveform has been removed. The major beat pulse peaks at orbital phase ~0.25, then shifts to earlier beat phases before reaching a minimum at orbital phase ~0.55.

the binary is given by

$$\Delta t = -\frac{d}{c}\sin(i)\cos(2\pi[\phi_{orb} - \phi_0]), \qquad (1)$$

where d is the distance of the emission from the binary center of mass, i is the orbital inclination, c is the speed of light, and ϕ_0 is orbital phase of inferior conjunction for the emitting material. Given the requirement that the emission originate on the donor (Marsh et al. 2016), the smallest-possible light-travel delay would occur for emission arising at the first Lagrangian point (L_1). If we adopt $M_1 = 0.8\,M_\odot$ and $M_2 = 0.3\,M_\odot$, as did Marsh et al. (2016), and assume an orbital inclination of $i = 60°$, then the semi-amplitude of the light-travel delay would be 0.6 s.

Although the effect of light-travel delays is relatively minor at our ~5 s cadence, a higher time resolution might potentially be able to discern light-travel delays from emission from different regions of the secondary (i.e., across a range of values of d and ϕ_0).

Although there might be a light-travel delay associated with the spin pulse, the region in which the optical spin pulse is generated is unknown, making it impossible to calculate its light-travel delay. Buckley et al. (2017) provide evidence that it might originate in a "striped wind" outside the light cylinder of the magnetosphere, which is almost an order of magnitude larger than the binary orbital separation.

4. Spin-down Ephemeris

4.1. Measuring the Spin-down

Marsh et al. (2016) detected a significant spin-frequency derivative of $\dot{\nu} = -(2.86 \pm 0.36) \times 10^{-17}\,\mathrm{Hz\,s^{-1}}$, implying a

Table 3
Beat-pulse Timings

Epoch[a]	T_{max} [BJD][b]	$T_{max,\,corr}$ [BJD][c]	±[days]
0	2457941.668881	2457941.668860	0.000008
1	2457941.670226	2457941.670210	0.000009
2	2457941.671584	2457941.671572	0.000011
3	2457941.672936	2457941.672930	0.000008
4	2457941.674330	2457941.674329	0.000010
5	2457941.675686	2457941.675691	0.000011
6	2457941.677076	2457941.677088	0.000008
7	2457941.678407	2457941.678427	0.000010
8	2457941.679758	2457941.679786	0.000010
9	2457941.681116	2457941.681153	0.000012

Notes.
[a] Relative to Equation (2).
[b] Raw pulse timings, uncorrected for orbital-phase dependence of arrival times.
[c] Pulse timings corrected for orbital phase.

(This table is available in its entirety in machine-readable form.)

spin-down of sufficient magnitude to power the optical pulsations. However, Potter & Buckley (2018) found that the Marsh et al. (2016) spin-down ephemeris did not accurately predict the frequencies observed in their power spectra and concluded their photometry was consistent with a constant spin period of 0.008538220(3) Hz, where the number in parentheses is the uncertainty on the final digit. While Potter & Buckley (2018) showed that the spin-down ephemeris from Marsh et al. (2016) was inaccurate, they noted that their results could still be reconciled with a nonzero $\dot{\nu}$ and that a longer baseline of observations was necessary to investigate this possibility.

Our results in Section 3 show that the beat pulse is more readily measured than the lower-amplitude spin pulse, so we use O−C measurements of the beat pulse to search for a change in the spin period. Assuming that any change in the orbital period is small over the baseline of observations, the derivative in the beat frequency will be a direct measure of the derivative of the spin frequency.

We measured 1077 beat-pulse timings[8] from our data set by fitting a Gaussian to each well-observed beat pulse. The timings, which span two years and three observing seasons, have a sufficiently long baseline to search for $\dot{\nu}$. We applied a correction to all pulse timings to compensate for the orbital-phase dependence of their arrival times, using the empirical fit from Figure 7. We then tested the Potter & Buckley (2018) linear ephemeris by computing an O−C diagram, using the beat period implied by their spin period. To improve the signal-to-noise ratio, we averaged the O−C residuals for each night and used the standard error of their mean as the 1σ uncertainty for each night. The residuals in this plot (Figure 8) show a rising trend, suggesting that the beat period inferred from Potter & Buckley (2018) is not a good match to our data. Further, there appears a significant curvature in the O−C measurements consistent with the presence of a period derivative.

We employed two independent fitting procedures—a bootstrap fit and an affine-invariant Markov Chain Monte Carlo algorithm (Foreman-Mackey et al. 2013)—to generate linear and quadratic ephemerides for the pulse maxima. We inspected the residuals from the linear and quadratic ephemerides

---

[8] These timings are available as an online table, and in Table 3, we provide a sample of them to illustrate the format of the data.
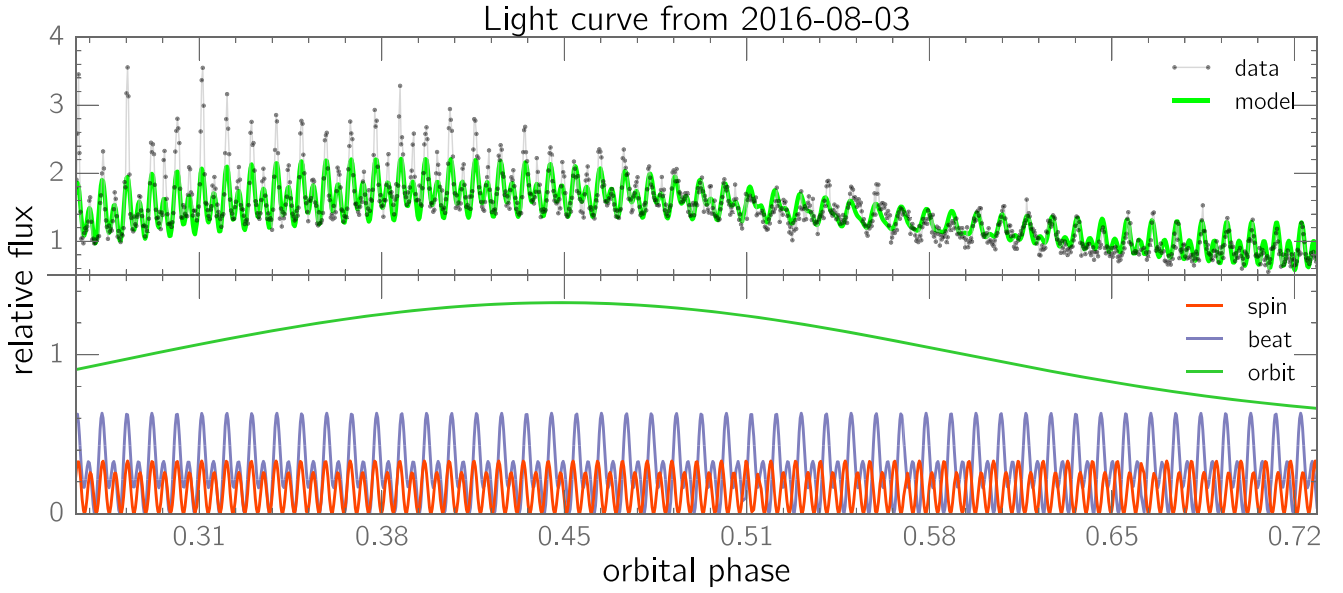
Figure 6. Top panel: an example of our data covering nearly half a binary orbit (points connected by a gray line). The thick line shows the light curve model combining a double-peaked beat pulse with a double-peaked spin pulse. Bottom panel: the three components used to build the model are an orbital modulation, the beat pulse, and the spin pulse. The spin and beat components each have two harmonic terms. The superposition of the spin and beat pulses causes the combined pulse profile to vary across the orbital period. This simple model accounts for the pulse amplitude and phase variations of over the orbit, but tends to underestimate the heights of the peaks over the brightest portion of the light curve.
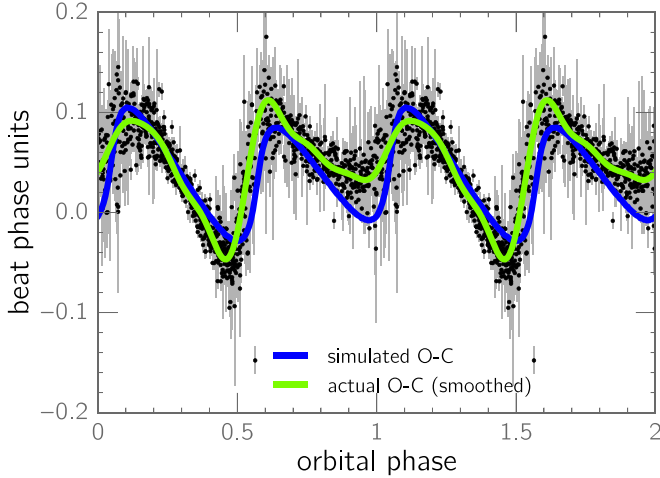
Figure 7. An O−C diagram of the beat pulses reveals an obvious orbital-phase dependence. The increased scatter in the residuals near orbital phase 0.5 corresponds with a dropoff in the amplitude of the beat pulse. Decreased S/N near orbital phase 0.0 contributes to the noisy timings near that phase.

(Figure 9) to determine which best described the data. While the measurements for each season systematically evade the linear fit, this trend vanished with the inclusion of a quadratic term, and the $\chi^2_{\rm red}$ statistic dropped from 13.1 to 2.6. Based on the quadratic fit, we calculate a beat ephemeris of

$$
\begin{aligned}
T_{\rm max}[{\rm BJD}] = {} & 4.91(31) \times 10^{-16}E^2 \\
& + 0.0013680458481(46)E \\
& + 2457941.6688507(36).
\end{aligned}
\tag{2}
$$

The quadratic coefficient is equivalent to $\frac{1}{2}\bar{P}_{\rm beat}\dot{P}_{\rm beat}$, where $\bar{P}_{\rm beat}$ is the average beat period, yielding a unitless period derivative of $\dot{P}_{\rm beat} = 7.18(45) \times 10^{-13}$. To convert this to a frequency derivative, we start with the definition $\nu = P^{-1}$ and differentiate with respect to P, obtaining $d\nu = -P^{-2}dP$. The
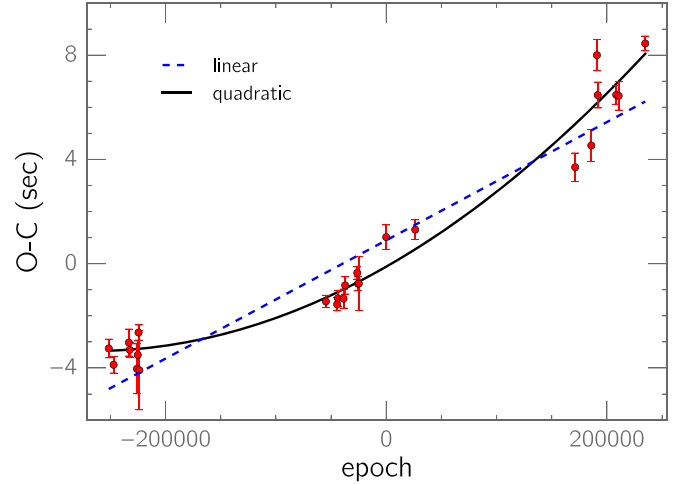

Figure 8. An O−C diagram of the SLKT beat-pulse timings using the Potter & Buckley (2018) beat period. Each point is the mean residual from a given observing run, and each errorbar is the standard error of that mean. A quadratic fit to the residuals yields a noticeably improved fit to the data compared to a simple linear fit, indicating that the measured O−C values are the result of a period derivative and not simply an inaccurate period.

time derivative of this relation is

$$
\dot{\nu} = -\frac{\dot{P}}{P^2}.
\tag{3}
$$

Thus, our $\dot{P}_{\rm beat}$ is equivalent to $\dot{\nu}_{\rm beat} = -5.14(32) \times 10^{-17}\,{\rm Hz\,s^{-1}}$.

4.2. Testing the Spin-down with AAVSO Photometry

Figure 9 includes O−C values from beat pulses in AAVSO photometry, but in order to provide an independent test of the spin-down ephemeris, these values were not included in the
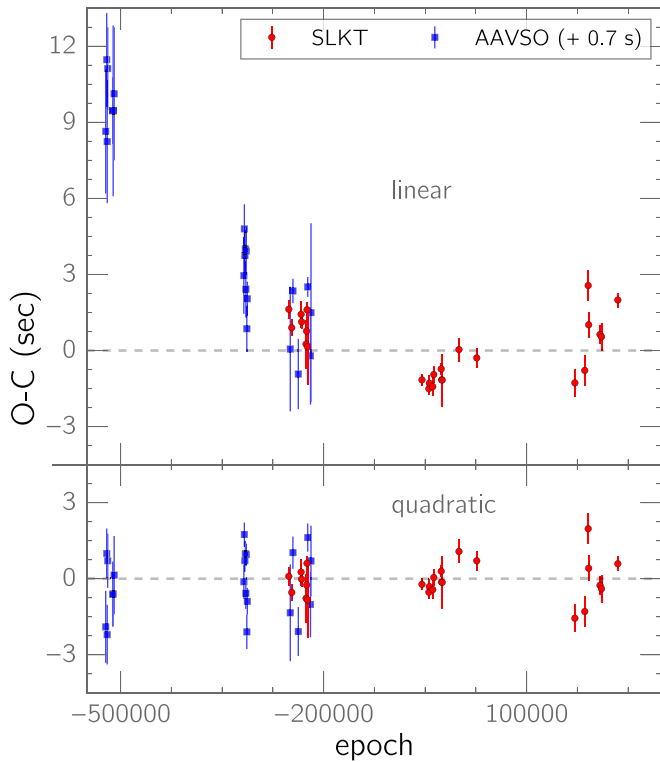
Figure 9. A comparison of the residuals from the best-fit linear and quadratic ephemerides to beat-pulse timings from the SLKT (red markers) and AAVSO data (blue markers). Only the SLKT data were used to generate the ephemerides; the AAVSO data are shown as an independent test of both fits. Each SLKT point gives the mean and standard error of the residuals from one observing run. As described in the text, a constant offset of 0.7 s was added to each AAVSO measurement to compensate for uncorrected shutter lag.

Figure 10. Top panel: a representative 1.2 hr section from a 5.7 hr AAVSO light curve whose image-to-image cadence was 24 s. Individual beat pulses are insufficiently resolved at this cadence for standard O−C analysis. The "CV" bandpass is unfiltered with a V zero point. Bottom panel: a phase plot of the beat pulse using the the full 5.7 hr light curve. The waveform of the beat pulse is sufficiently well-sampled that its phase of maximum light can be measured. The red markers are phase bins.

calculation of Equation (2). Because the cadences of these time series were too slow for O−C analysis of individual beat maxima, we took each AAVSO light curve and phased it to the beat period using our linear and quadratic ephemerides. The resulting beat-phase plots, an example of which is shown in Figure 10, can be used to measure the average phase of the beat-pulse maxima provided that enough beat cycles were observed. We filtered the AAVSO photometry to exclude any time series with a cadence slower than 35 s or a duration shorter than 1 hr, and we applied a correction for the orbital-phase dependence of the pulse arrival times. We further excluded any time series afflicted by aliasing between the beat period and the observing cadence.

With the benefit of the extended baseline of observations, it is immediately obvious in Figure 9 that the linear ephemeris leads to strong curvature in the residuals. By contrast, the quadratic residuals do not show any systematic trend.

No shutter-lag correction was applied to the AAVSO data, and the raw AAVSO quadratic residuals showed an offset of −0.7 s with respect to contemporaneous SLKT residuals. An uncorrected shutter lag will cause timestamps to be earlier than the data that they describe, imparting a small, negative O−C to the pulse timings. We therefore attribute the constant, negative offset of the AAVSO residuals to uncorrected shutter lag, and in Figure 9, we add an offset of 0.7 s to each AAVSO residual to compensate for this effect. Regardless of the cause of this offset, the lack of a systematic trend in the AAVSO quadratic residuals supports our measurement of the spin-down.
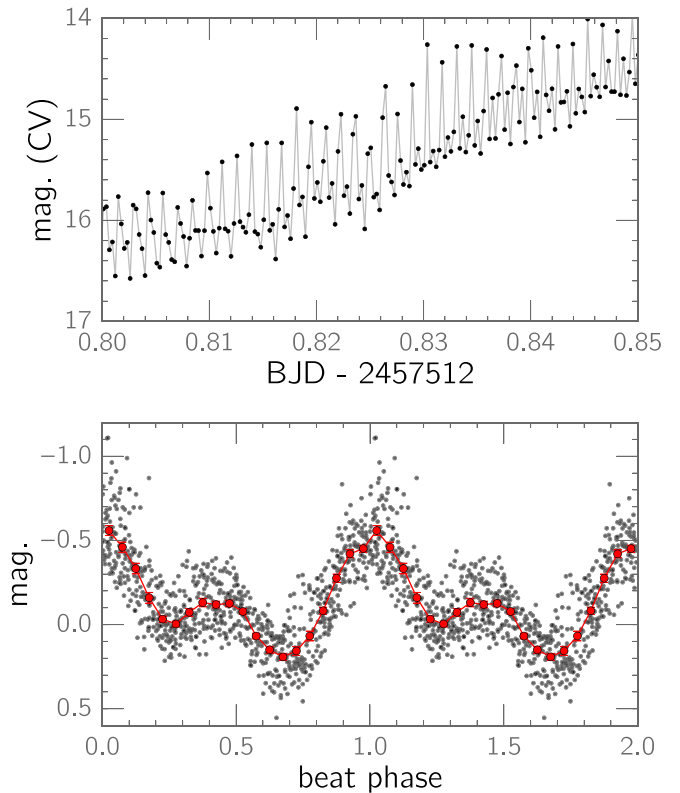
4.3. The Nature of $\dot{\nu}_{\rm beat}$

Because the beat frequency is defined as $\nu_{\rm beat} = \nu_{\rm spin} - \nu_{\rm orb}$, its time derivative is $\dot{\nu}_{\rm beat} = \dot{\nu}_{\rm spin} - \dot{\nu}_{\rm orb}$, meaning that the observed $\dot{\nu}_{\rm beat}$ could be caused either by a decrease of the spin frequency or an increase in the orbital frequency. If the orbital period were changing so rapidly, there would be detectable consequences in long-term photometry. To explore this possibility, we used phase-dispersion minimization (PDM; Stellingwerf 1978) to determine whether an increasing orbital frequency could reduce the scatter in orbital phase plots using 13 years of survey photometry from the Catalina Real-Time Transient Survey (CRTS; Drake et al. 2009) and All-Sky Automated Survey for Supernovae (ASAS-SN; Shappee et al. 2014; Kochanek et al. 2017). For a range of $\dot{\nu}_{\rm orb}$ between 1×10^{-19} and $1 \times 10^{-16}\,{\rm Hz\,s^{-1}}$, we phased the survey photometry using a quadratic orbital ephemeris in which we assumed an initial orbital period of $P_0 = 0.14853528$ days (Marsh et al. 2016) at an epoch of JD = 2455000.5 (Potter & Buckley 2018).[9] For each quadratic phase plot, we computed the PDM statistic and normalized it to the the PDM statistic for the phase plot constructed with the linear ephemeris from

---

[9] This is the epoch of the CRTS photometry used by Marsh et al. (2016) to measure the orbital period. It is different than the epoch in the orbital ephemeris in Marsh et al. (2016), which reported a spectroscopically determined epoch and assumed—correctly—that the orbital period did not change appreciably in the intervening 5 years since the CRTS epoch. Phase plots using the CRTS epoch will have a uniform horizontal offset with respect to the Marsh et al. (2016) epoch, but this does not impact our PDM analysis.
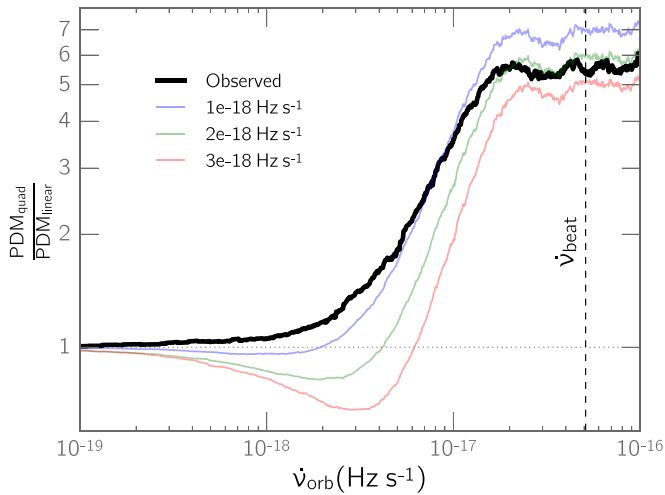
Figure 11. PDM analysis showing the effect of an increase in the orbital frequency across 13 years of CRTS and ASAS-SN photometry (thick black line). For each value of $\dot{\nu}_{orb}$, we calculated a quadratic orbital ephemeris, computed the PDM statistic of the resulting phase plot, and normalized it to the PDM statistic of the linear-ephemeris phase plot. A value greater than 1 (dotted horizontal line) indicates that adding $\dot{\nu}_{orb}$ increases the scatter in the phase plot, while values less than 1 indicate that $\dot{\nu}_{orb}$ reduces the scatter. The colored lines show the results of simulations in which an artificial $\dot{\nu}_{orb}$ was injected into a model of the orbital light curve. For $\dot{\nu}_{orb} \geqslant 2 \times 10^{-18}$ Hz s^{-1}, our technique successfully recovers the simulated $\dot{\nu}_{orb}$ at the global minimum of a given curve. We therefore conclude that $\dot{\nu}_{orb} < \sim 2 \times 10^{-18}$ Hz s^{-1} and is too small to account for the observed $\dot{\nu}_{beat}$ (dashed vertical line).

Marsh et al. (2016). The results of this analysis are shown in Figure 11. For $\dot{\nu}_{orb} > 2 \times 10^{-18}$ Hz s^{-1}, the phase plots contain an obvious increased scatter with respect to the linear ephemeris; below that value, the effect of $\dot{\nu}_{orb}$ becomes negligible, so we constrain $\dot{\nu}_{orb} < \sim 2 \times 10^{-18}$ Hz s^{-1}. To verify this constraint, we created a simulated orbital light curve of AR Sco, injected an artificial $\dot{\nu}_{orb}$, and matched the sampling of the simulated data to the actual observations. As Figure 11 shows, our algorithm successfully recovered values of $\dot{\nu}_{orb}$ in excess of 2×10^{-18} Hz s^{-1}, but below that threshold, it could not discern the simulated $\dot{\nu}_{orb}$, bolstering our constraint.

The non-detection of $\dot{\nu}_{orb}$ is consistent with the measurements of the orbital phase of maximum light from Littlefield et al. (2017). An increasing orbital frequency (i.e., $\dot{P}_{orb} < 0$) would induce concave-down curvature in their Figure 4, but this is not seen. We conclude, therefore, that any $\dot{\nu}_{orb}$ contributes negligibly to $\dot{\nu}_{beat}$, such that $\dot{\nu}_{beat} = \dot{\nu}_{spin}$ to within our measurement uncertainty. Thus, the subscript notation becomes unnecessary for $\dot{\nu}$.

Because we have established that $\dot{\nu}$ is the same for the spin and beat frequencies, we can directly compare our measurement of $\dot{\nu}$ with its counterpart from Marsh et al. (2016). Our estimate is larger by a factor of ~ 1.8, but it still satisfies the constraint from Potter & Buckley (2018) that $\sim -2 \times 10^{-16}$ Hz s$^{-1} < \dot{\nu} < \sim 1 \times 10^{-16}$ Hz s^{-1}.

4.4. Reconciling Marsh et al. (2016) with Potter & Buckley (2018)

The disagreement between the Marsh et al. (2016) spin-down ephemeris and the measured spin frequency in Potter & Buckley (2018) provides a stringent test of our spin-down ephemeris. In Figure 12, we plot the extrapolated beat period from Equation (2) as a function of beat-cycle count, overlaying the beat periods from both Marsh et al. (2016) and Potter &
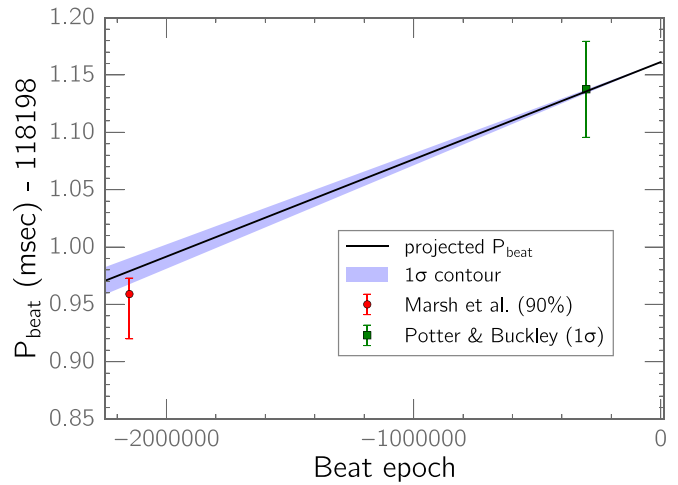

Figure 12. Projected beat period using Equation (2). The two markers indicate the beat periods reported by Marsh et al. (2016) and Potter & Buckley (2018). Since Potter & Buckley (2018) did not explicitly provide a beat period, we calculated it from their spin period and the Marsh et al. (2016) orbital period. As indicated in the legend, Marsh et al. (2016) reported a 90% confidence interval for their result, while Potter & Buckley (2018) provided a 1σ interval. Even though these two points were not considered in the fitting procedure for Equation (2), the projected beat period is in excellent agreement with both measurements, substantiating our measurement of the WD's spin-down.

Buckley (2018) at the appropriate epochs.[10] Even though our beat ephemeris was calculated without regard to either of these two measurements, the projected beat period is in excellent agreement with both measurements. Furthermore, the difference between the Potter & Buckley (2018) and Marsh et al. (2016) spin frequencies, when divided by the difference in epochs yields $\dot{\nu} = -(5.9 \pm 1.5) \times 10^{-17}$ Hz s^{-1}, consistent with both our measurement ($\dot{\nu} = -5.14(32) \times 10^{-17}$ Hz s^{-1}) and the constraints from Potter & Buckley (2018).

This suggests that the inability of the Marsh et al. (2016) ephemeris to correctly predict the spin and beat frequencies in Potter & Buckley (2018) is a consequence of an underestimated $\dot{\nu}$ and can be remedied by using our measurement of the spin-down. Despite the error in their estimate of $\dot{\nu}$, it is remarkable, given the sparse sampling and comparatively low time resolution of the survey photometry available to them, that they were able to accurately measure ν_{orb}, ν_{beat}, and ν_{spin} while also estimating $\dot{\nu}$ to within a factor of 2.

4.5. Spin-down Luminosity

Our precise measurement of the frequency decay rate allows us to improve the estimate of the spin power available for conversion into the observed electromagnetic (EM) energy. The spin-down luminosity, is given by $L_{\dot{\nu}} = -4\pi^2 I \nu_{spin} \dot{\nu}$, where I is the WD's moment of inertia (Marsh et al. 2016). As did Marsh et al. (2016), we assume a 0.8 $M_\odot$ WD with a radius of 0.01 $R_\odot$. The mass–radius relation for non-relativistic WD stars means that the moment of inertia changes as $I \propto M^{1/3}$, and is rather insensitive to variations in the assumed mass. In the non-relativistic regime, WDs are predicted to have a density structure like that of a polytrope with an index of 1.5, and we calculate a moment of inertia of $I = 0.25MR^2 = 2 \times 10^{43}$ kg m^2. However, the strong magnetic fields and the rapid

---

[10] Potter & Buckley (2018) reported only ν_{spin}, so we used ν_{orb} from Marsh et al. (2016) to calculate the corresponding ν_{beat}.

spin rate of the WD may have an effect on the precise value of the moment of inertia (Franzon & Schramm 2017).

Thus, we find the spin-down power is 3×10^{26} W. The *Gaia* DR2 parallax (Gaia Collaboration et al. 2016, 2018) to AR Sco (8.492 ± 0.041 mas) is equivalent to a distance of 117.8 ± 0.6 pc, which is close enough to the Marsh et al. (2016) value that it is unnecessary to correct their measurement of the average EM power of the pulsations. We find the efficiency of converting the spin energy to detected EM emission to be $\sim 4\%$.

5. Conclusion

The complex morphological variations seen in the optical light curve of AR Sco are explained as the superposition of the spin and beat pulses, as well as a slower orbital modulation. As noted in earlier studies, a beat cycle consists of a major and minor pulse. Here, we show the minor pulse has half the amplitude of the brighter signal after removing contamination from the spin pulse. We find the spin cycle also consists of two distinct pulses, but their amplitudes are comparable. The major spin pulse is half the amplitude of the major beat pulse and therefore, about the same amplitude as the minor beat pulse.

Over an orbit, the major beat and spin pulses add constructively between phases 0.2 and 0.3, resulting in the highest-amplitude optical variations observed in the system. Half an orbit later, the major beat and minor spin pulses add together along with the minor beat and major spin pulses. This combination results in lower amplitude peaks when compared with orbital phases around 0.25. The smallest amplitudes are seen when the beat and spin pulses are out of phase and destructively interfere around orbital phases between 0.5 and 0.6. This model provides a good overall fit to the rapid variations seen in AR Sco. We also show that this model explains the O−C variations seen in the timings of the beat pulses.

Our simple model assumes constant beat and spin amplitudes over an orbit, and this does not fully match the largest amplitudes fluctuations observed around orbital phases 0.2–0.4. A more complete model would take into account the changing viewing angle of the secondary star thought to be the origin of the beat emission.

The major beat and spin pulses coincide at orbital phase 0.3, resulting in the highest-amplitude peaks in the AR Sco light curve. The beat pulse likely comes from near the surface of the red secondary star (Marsh et al. 2016), while the spin pulse is likely originating in the magnetic field of the WD. If we assume that beat maxima occur when one of the WD magnetic poles is pointing toward the secondary, then the geometry of the system suggests that we see the peak spin pulse when the WD magnetic pole is nearly perpendicular to our line of sight.

Perhaps most importantly, our results establish that the WD is indeed spinning down (as originally proposed by Marsh et al. 2016), but the frequency derivative that we measure is almost twice as large as their estimate. Our updated spin-down

ephemeris successfully passes two tests: it accurately predicts the evolution of the beat period between the Marsh et al. (2016) and Potter & Buckley (2018) epochs, and it also accounts for the pulse-arrival times in AAVSO photometry. Furthermore, it comports with the constraints on the spin-down rate established in Potter & Buckley (2018). Our measurement of the spin-down of the WD confirms the conclusion by Marsh et al. (2016) that the pulsed EM emission from AR Sco can be powered by the rotational energy of the WD.

ORCID iDs

Robert A. Stiller ⓘ https://orcid.org/0000-0002-7181-2554
Colin Littlefield ⓘ https://orcid.org/0000-0001-7746-5795
Peter Garnavich ⓘ https://orcid.org/0000-0003-4069-2817
Charlotte Wood ⓘ https://orcid.org/0000-0003-4773-4602
Gordon Myers ⓘ https://orcid.org/0000-0002-9810-0506

References

Astropy Collaboration, Robitaille, T. P., Tollerud, E. J., et al. 2013, A&A, 558, A33
Buckley, D. A. H., Meintjes, P. J., Potter, S. B., Marsh, T. R., & Gänsicke, B. T. 2017, NatAs, 1, 29
Drake, A. J., Djorgovski, S. G., Mahabal, A., et al. 2009, ApJ, 696, 870
Foreman-Mackey, D., Hogg, D. W., Lang, D., & Goodman, J. 2013, PASP, 125, 306
Franzon, B., & Schramm, S. 2017, MNRAS, 467, 4484
Gaia Collaboration, Brown, A. G. A., Vallenari, A., et al. 2018, arXiv:1804.09365
Gaia Collaboration, Prusti, T., de Bruijne, J. H. J., et al. 2016, A&A, 595, A1
Geng, J.-J., Zhang, B., & Huang, Y.-F. 2016, ApJL, 831, L10
Katz, J. I. 2017, ApJ, 835, 15
Kochanek, C. S., Shappee, B. J., Stanek, K. Z., et al. 2017, PASP, 129, 104502
Littlefield, C., Garnavich, P., Kennedy, M., et al. 2017, ApJL, 845, L7
Littlefield, C., Garnavich, P., Kennedy, M. R., et al. 2016, ApJ, 833, 93
Marsh, T. R., Gänsicke, B. T., Hümmerich, S., et al. 2016, Natur, 537, 374
Osborne, J., & Mukai, K. 1989, MNRAS, 238, 1233
Patterson, J. 2012, JAVSO, 40, 240
Potter, S. B., & Buckley, D. A. H. 2018, MNRAS Letters, 478, L78
Shappee, B. J., Prieto, J. L., Grupe, D., et al. 2014, ApJ, 788, 48
Stanway, E. R., Marsh, T. R., Chote, P., et al. 2018, arXiv:1801.07258
Stellingwerf, R. F. 1978, ApJ, 224, 953
Takata, J., Hu, C.-P., Lin, L. C. C., et al. 2018, ApJ, 853, 106